ACS APPLIED MATERIALS & INTERFACES

Research Article

www.acsami.org

n-Type Carbon Nanotubes/Silver Telluride Nanohybrid Buckypaper with a High-Thermoelectric Figure of Merit

Weiyun Zhao,[†] Hui Teng Tan,[†] Li Ping Tan,[†] Shufen Fan,[†] Huey Hoon Hng,[†] Yin Chiang Freddy Boey,[†] Igor Beloborodov,[‡] and Qingyu Yan*[,†]

[†]School of Materials Science and Engineering, Nanyang Technological University, Singapore 639798, Singapore

[‡]Department of Physics and Astronomy, California State University Northridge, 18111 Nordhoff Street, Northridge, California 91330, United States

Supporting Information

ABSTRACT: n-Type thermoelectric (TE) materials was made from carbon nanotube (CNT) buckypapers. We used silver telluride (Ag_2Te) to achieve electron injection to the CNTs. The TE characterizations on more than 50 samples show that the CNTs/Ag_2Te hybrids exhibit negative Seebeck coefficients (e.g., n-type) from −30 to −228 μV/K. Meanwhile, the tunneling coupling between the CNTs and Ag_2Te increase the electrical conductance to the range of 10 000−20 000 S/m, which is higher than each single component (CNTs or Ag_2Te). These n-type TE buckypapers are flexible and robust with ZT values of 1−2 orders of magnitude higher than previously reproted for CNT-based TE materials. In addition, the preparation of such buckypapers are very simple compared to a tranditonal inorganic process, without the need for hot pressing or spark sintering. These n-type TE buckypapers can provide important components for fabricating CNT-based flexible TE devices with good conversion efficiency.

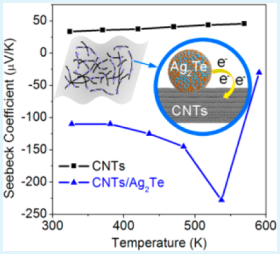

KEYWORDS: *carbon nanotube, silver telluride, thermoelectric, figure of merit, Seebeck, flexible*

INTRODUCTION

In the past few decades, thermoelectric (TE) materials have achieved great enhancements in converting waste heat to power.[1,2] The efficiency of TE materials, figure of merit, ZT, can be expressed as $ZT = S^2\sigma T/\kappa$, where S is the Seebeck coefficient, σ is the electrical conductivity, T is the absolute temperature, and κ is the thermal conductivity. To obtain advanced efficiency of TE materials, a high Seebeck coefficient, high electrical conductivity, and low thermal conductivity are required. Many efforts on enhancing TE performances in recent years are nanostructuring the materials and, hence, significantly decreasing the thermal conductivity.[3−6] Thus far, most of the advanced TE materials are reported on inorganic crystals,[7−13] which are rigid and brittle. Many times, the TE devices made from these inorganic crystals may be subjected to failure under continuous thermal cycling because of the mismatch of the thermal expansion among different components. Some strategies have been developed to solve this issue. For example, it has been reported that carbon nanotubes can be used as the interface material to combine with Bi_2Te_3 to improve the thermomechanical compliance.[14] Development of flexible TE materials is another attractive approach. Organic materials, such as conducting polymers, were reported as flexible TE materials.[15] However, those materials often have low electrical conductivity (<500 S/m), which leads to a low ZT value.[16,17] Also, it may be difficult to expand their application into the high-temperature range, e.g., >500 K.[18]

A carbon nanotube (CNT) has many advantages, such as chemically stable,[19,20] highly electrically conductive,[21,22] and mechanically robust.[23,24] Owning to these advanced properties as well as abundance of carbon on the Earth, CNT is an important candidate to build flexible electronics.[25−27] However, it is seldom regarded as a TE material because of its poor Seebeck coefficient (<60 μV/K)[28] and high thermal conductivity of a single tube (~250−10 000 W m^{-1} K^{-1} for single tube or aligned arrays).[29−31] It has been reported that low thermal conductivities can be obtained in CNTs/conductive polymer composites and processed tubes.[32] For example, combining CNTs with polyaniline can reduce thermal conductivity to ~0.5 W m^{-1} K^{-1}.[33] Also, in our previous reported work, plasma-treated CNT buckypaper shows attractive p-type Seebeck values of ~350 μV/K, while the electrical conductivity still maintains an acceptable value (~1000 S/m).[34] Hence, CNT-based materials still hold the promising potential to achieve TE properties comparable to some of the reported traditional inorganic materials, such as BiSbTe[35,36] or PbTe.[37−39] On the basis of reported literature, more studies on p-type behavior were reported for TE measurement of CNT-related samples.[40−43] Thus far, although there are a few works on n-type CNT-related materials, either a low Seebeck value[44,45] or a low electrical conductivity[46] is obtained and only low ZT values of ~10^{-3} are achieved.[47] Hence, more efforts should be performed to achieve ZT to an acceptable value (e.g., > 0.1), which is comparable to traditional

Received: December 26, 2013
Accepted: March 19, 2014
Published: March 19, 2014

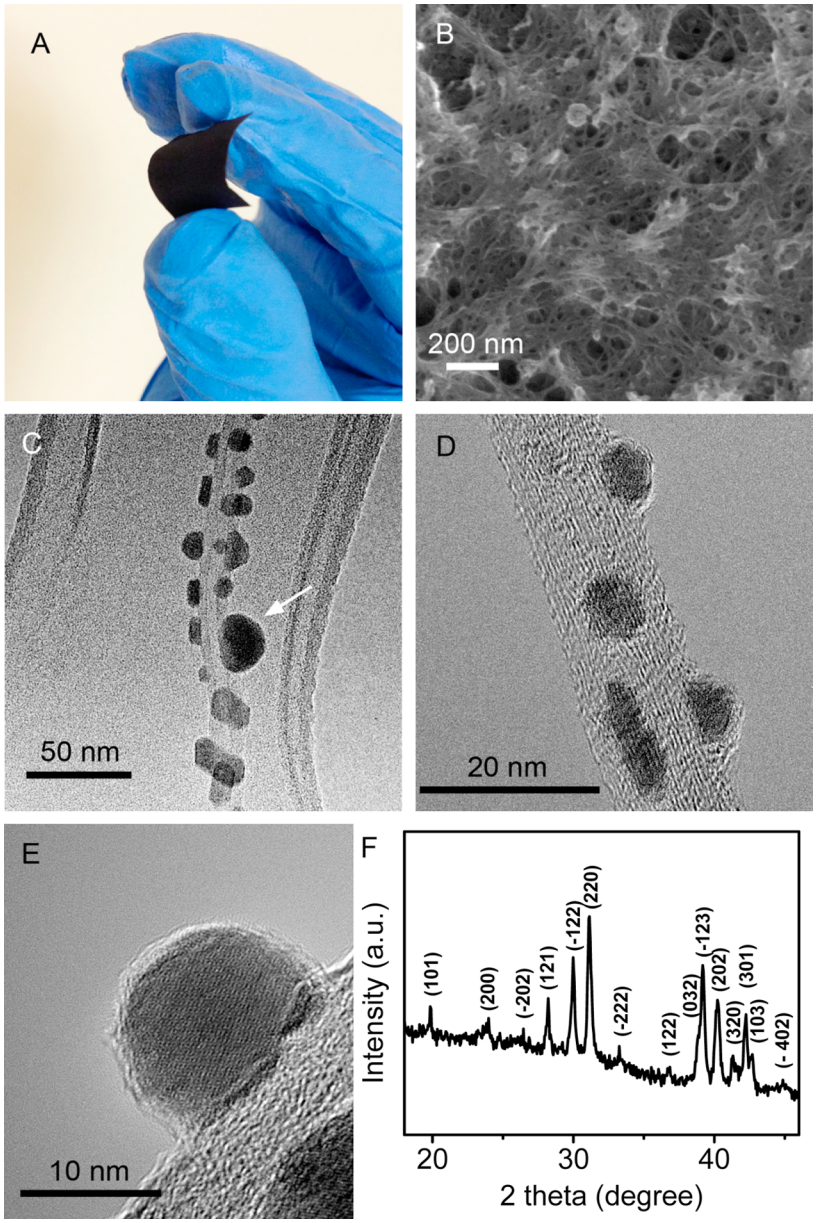

Figure 1. (A) Optical image, (B) FESEM image, (C and D) TEM images, (E) HRTEM image, and (F) XRD pattern of the CNTs/Ag_2Te hybrid.

inorganic materials. Development of such n-type TE materials is encouraging to provide important components for fabricating CNT-based flexible TE devices.

Herein, we report the preparation of n-type TE materials of silver telluride (Ag_2Te)-decorated single-walled carbon nanotubes (SWCNTs; Sigma-Aldrich; carbon > 90%; ≥77% carbon as SWCNT) (CNTs/Ag_2Te). The sample was prepared via an oil-phase step and then processed into flexible buckypapers. The size of the Ag_2Te particle is around 10 nm. The mass ratio between CNTs and Ag_2Te can be easily tuned by varying the precursor ratio. The TE characterizations on more than 50 samples show that the CNTs/Ag_2Te hybrids exhibit negative Seebeck coefficients (e.g., n-type) from −30 to −228 μV/K. The electrical conductivity increases for samples with higher amounts of Ag_2Te and can reach the range of 10 000−20 000 S/m. The measured thermal conductivity for such hybrid buckypapers can be as low as ∼0.7 W m^{-1} K^{-1} in the temperature range of 325−525 K. If we do not consider the anisotropic aspect of such buckypaper (e.g., this assumption allows us to calculate the figure of merit, *ZT*, based on the measured electric conductivities, Seebeck coefficients, and thermal conductivities), the estimated highest figure of merit, *ZT*, of CNTs/Ag_2Te hybrids was 0.44 (±5%) at 525 K. Such a *ZT* value is comparable to some of the traditional TE materials and is higher than that of either pristine CNT or pure Ag_2Te.

EXPERIMENTAL SECTION

Synthesis. In a typical synthesis, silver precursor was first prepared by 170 mg (1 mmol) of $AgNO_3$ dissolving in 10 mL of deionized (DI) water in a flask. Then, 10 mL of toluene with 0.24 mL (1 mmol) of 1-dodecanethiol was added to the solution and well-stirred for 1 h at room temperature for ligand attachment. After that, the stirring was stopped and the solution was self-divided into two phases. Next, the clear aqua phase at the bottom of the flask was removed. The CNTs (1, 3, and 5 mg) were dispersed in toluene via 2 h of ultrasonication. Then, the well-dispersed CNTs were added to the silver precursor solution first. The temperature was increased to 383 K and maintained for 10 min or so. After that, 0.5 mL of TOP-Te solution (1 M) was injected into the as-prepared solution and stirred for 2 min at 383 K.

dx.doi.org/10.1021/am4059167 | ACS Appl. Mater. Interfaces 2014, 6, 4940−4946

The 1 M TOP-Te solution was prepared via dissolving 1.276 g of Te powder into 10 mL of trioctylphosphine. After 2 min of reaction, the flask was quickly quenched in cold water. Next, the sample solution was further dissolved in hexane and then washed by ethanol 2−3 times. The washed solutions were dropped cast onto copper foils and dried in the oven with the temperature of 333 K. After the solvent evaporated, the Ag_2Te/CNT sheets were self-peeled off from the copper foils. To remove the −thiol capping on the samples, the samples were annealed in Ar at 673 K for 1 h. For the Ag_2Te sample, because it was not flexible enough to make a free-standing sheet, the powder was collected and hot-pressed into a pellet in Ar at 673 K.

Characterization Techniques. The morphology and nanostructures of the samples were characterized using X-ray diffraction (XRD; Bruker D8 Powder), field emission scanning electron microscopy (FESEM; JEOL JSM7600), and transmission electron microscopy (TEM; JEOL JEM-2100F). The TEM samples were prepared by dropping the solutions onto copper grids and annealing the whole copper grid in Ar at 673 K. The Hall measurement was carried out using Hall system HL 5500 at room temperature under the van der Pauw mode. The Seebeck coefficient and resistivity were measured from 323 to 523 K using the ZEM-3 Seebeck meter under a helium environment (see Figure S1 of the Supporting Information). The samples were cut into a rectangular piece with a dimension of 10 × 4 mm^2 and fixed on a glass substrate by applying silver paste to both ends. The samples for thermal conductivity measurements were cut into 12.7 × 12.7 mm^2 (CNTs/Ag_2Te hybrid and pure CNT buckypaper) or polished into the round pellet with the diameter of 12.7 mm (Ag_2Te pellet) and were measured by laser flash (NETZSCH MicroFlash LFA457).

RESULTS AND DISCUSSION

Five types of samples, including pure Ag_2Te, pure CNTs, and three CNTs/Ag_2Te hybrids, were prepared for characterization and TE property measurements. The CNTs/Ag_2Te hybrid samples were prepared by injecting TOP-Te into oil-phase solution containing Ag precursor, CNT, and surfactant 1-dodecanethiol. The weight ratios of CNT Ag_2Te can be adjusted by changing the amount of CNT and estimated on the basis of the amount of precursor added. The estimated weight ratios of CNT/Ag_2Te of three hybrid composites were 1:17, 3:17, and 5:17 and named as CA-1, CA-2, and CA-3, respectively. Figure 1A is the optical image of the buckypaper of sample CA-1. It was prepared via drop casting the washed CNTs/Ag_2Te hybrid solution onto copper foil and peeling off the free-standing paper after drying. The buckypapers were then annealed at 673 K. The obtained buckypaper was around 50 μm in thickness and mechanically robust upon repeated bending. The low-magnification FESEM image of hybrid sample CA-1 (Figure 1B) indicates that the CNT bundles were entangled randomly. Panels C−E of Figure 1 are transmission electron microscopy (TEM) images that show the morphology and structure of the hybrid sample CA-1. It can be found that most Ag_2Te particles attached on the CNT walls are around 10 nm. Small particles may agglomerate and form large particles during the annealing process. One large particle of around 25 nm, which is denoted by the arrow, can also be observed (Figure 1C). Additionally, we can find that the diameter of a single CNT is <1 nm, but the CNTs may self-assemble into bundles (Figure 1D) because of the van der Waals force. The diameters of CNT bundles shown in panels C and D of Figure 1 are around 10 nm. Figure 1E is a high-resolution TEM (HRTEM) image of an Ag_2Te particle on CNT walls. It indicates that the Ag_2Te particle is single-crystalline. The representative XRD pattern of CA-1 is shown in Figure 1F, which matches the monoclinic Ag_2Te phase [Joint Committee on Powder Diffraction Standards (JCPDS) number 34-0142]. There is no detectable impurity phase.

For comparison purposes, pure Ag_2Te and pure CNT samples were also prepared. Ag_2Te was synthesized by a similar method as that of CNTs/Ag_2Te hybrids but without adding CNTs. Figure 2A shows the XRD pattern of pure Ag_2Te. Peaks

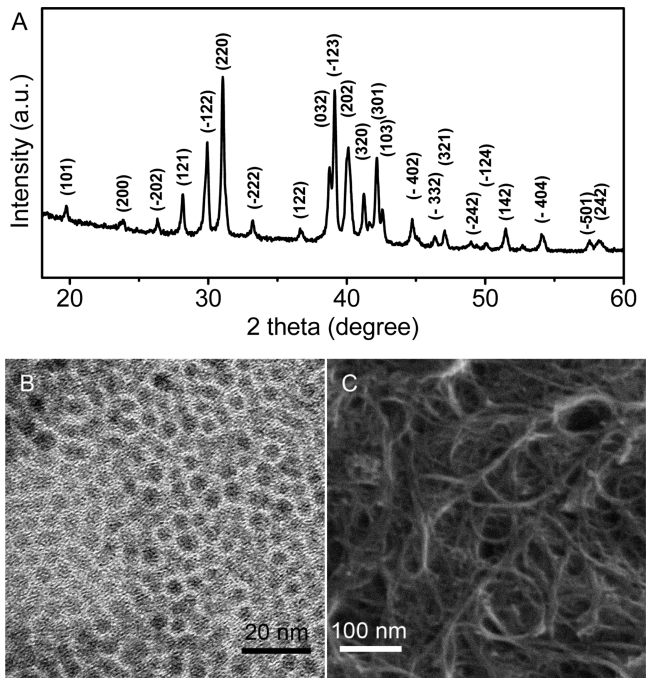

Figure 2. (A) XRD pattern of pure Ag_2Te. (B) TEM image of pure Ag_2Te nanoparticles. (C) SEM image of pure CNT random networks.

corresponding to the monoclinic Ag_2Te phase (JCPDS number 34-0142) can be observed. There is a reversible phase transition of Ag_2Te at 418 K from the β phase with a monoclinic structure to the α phase with a face-centered cubic (fcc) structure. Although the samples were annealed at 673 K after synthesis, no impurity phase, except for the monoclinic Ag_2Te phase, is detectable according to the XRD result. Thus, we believe that Ag_2Te can be easily converted back from the fcc phase to the monoclinic phase when the temperature returns to lower temperatures (<418 K). Figure 2B shows the TEM image of pure Ag_2Te particles. The nanoparticles are uniform with the size of ∼5 nm. Figure 2C is the FESEM image of pure CNT buckypaper. It shows a random network of CNT bundles. The average diameter of CNT bundles is around 10 nm.

For TE property measurements, CNTs/Ag_2Te hybrid buckypapers with a thichness of ∼50 μm were cut into proper size for different measurements. Pure CNTs were also prepared into flexible buckypaper for TE measurements. Pure Ag_2Te was rigid and brittle; therefore, it cannot be prepared into a free-standing sheet. Hence, the Ag_2Te pellet was prepared via hot press at 673 K.

Electrical conductivity values of three CNTs/Ag_2Te hybrid buckypapers (CA-1, CA-2, and CA-3) are shown in Figure 3A. It shows that samples with a higher Ag_2Te content exhibit higher electrical conductivities at the same temperature range. CA-1 shows the highest electrical conductivity of 23 500 S/m at 381 K. The shape of the electrical conductivity curves are similar for these three samples within the measurement temperature of 325−550 K. The electrical conductivity of

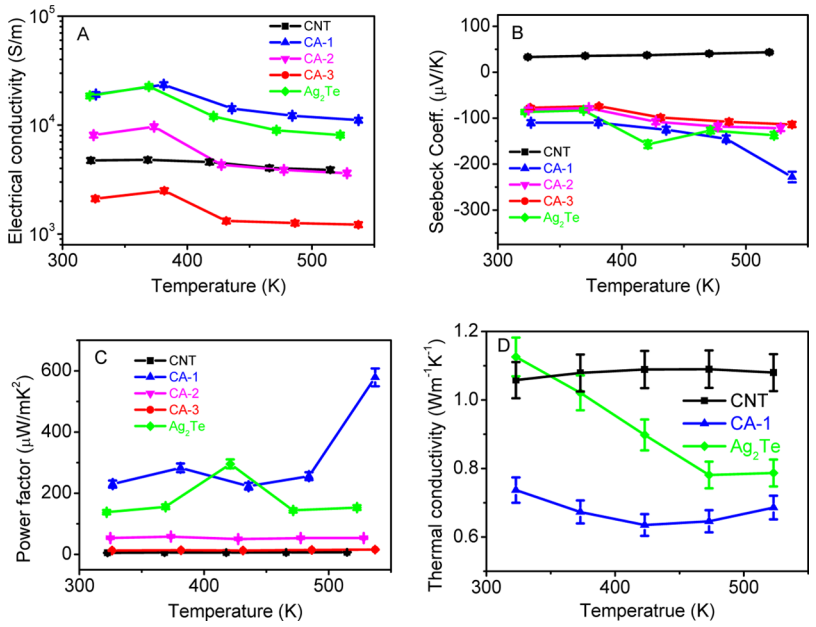

Figure 3. (A) Electrical conductivity, (B) Seebeck coefficient, (C) power factor, and (D) thermal conductivity of CNTs/Ag_2Te hybrid buckypapers, pure Ag_2Te pellet, and pure CNT buckypaper.

CNTs/Ag_2Te hybrids drops suddenly at a temperature close to the phase transition point of Ag_2Te (i.e., 418 K). Below the phase transition point, the electrical conductivity becomes higher at an increased temperature, which shows a typical semiconducting behavior. At a temperature range of $T > 418$ K, the electrical conductivity decreases with the increase of the temperature, which becomes a metallic/heavily doped semiconducting behavior. A pure Ag_2Te pellet and pure CNT buckypaper were also measured for comparison. The electrical conductivity curve of the pure Ag_2Te pellet displays a similar trend to that of CNTs/Ag_2Te hybrids. It increases at an increased temperature below the phase transition point and decreases at an increased temperature above the phase transition point. The electrical conductivity of CNT buckypaper is 3500−5000 S/m in the measured temperature range. It decreases at increased temperatures, which shows a metallic/heavily doped semiconducting behavior. The electrical conductivity of CA-1 is higher than both pure CNT buckypaper and pure Ag_2Te pellet, which shows the synergism in the CNTs/Ag_2Te hybrid structure similar to the previous reported effect for binary nanocrystal superlattices.[48] The higher electrical conductivity of CA-1 compared to pure CNT buckypaper is possibly related to the doping effect. The electrical properties of all CNTs/Ag_2Te hybrid samples and the pure Ag_2Te pellet can be further studied with Hall measurements at room temperature (Table 1). The mobility, μ, can be calculated via $\sigma = n\mu e$, where σ is the electrical conductivity, n is the carrier concentration, and e is the elementary charge. For the three CNTs/Ag_2Te hybrids, the carrier concentration is higher for samples with more Ag_2Te. The sample CA-1, which contains most Ag_2Te, has the largest carrier concentration of 6.591×10^{18} cm^{-3} among the three CNTs/Ag_2Te hybrids. This observation indicates that, during the Ag_2Te decoration process, electrons are injected from Ag_2Te to CNTs. With the increase of the Ag_2Te content, more electrons exist in the system; hence, the carrier concentration increases. The mobilities of CNTs/Ag_2Te hybrids show a non-monotonic trend. This is because of the fact that, in these hybrid samples, Ag_2Te plays multiple roles, including network element, electron donor, impurity, etc. Therefore, their impact on the electronic properties is complex. For example, as network elements, they provide extra transport channels, helping to enhance electron mobility, while those decorated onto CNTs scatter electrons. Thus, a combination of these interactions between composites and carriers possibly gives rise to a non-monotonic mobility trend.[49,50] Additionally, we found that the mobilities of CNTs/Ag_2Te hybrids (120−250 $cm^2\ V^{-1}\ s^{-1}$) are higher than pure Ag_2Te (12.702 $cm^2\ V^{-1}\ s^{-1}$) by 1 order of magnitude. Although the electron scattering caused by the CNTs/Ag_2Te interfaces may be stronger than the Ag_2Te/Ag_2Te interfaces, the change of the electron mean free path (MFP) should also be considered. Because Ag_2Te is a nanoparticle, the electron MFP in Ag_2Te is shorter than the size of the particle (i.e., 10 nm) and electron transport is limited by the size of the nanoparticle. However, MFP can be much longer in CNTs, considering the length of CNTs (hundreds of nanometers to several micrometers) and their exotic transport property along the tube. Thus, in hybrid samples, the average MFP is enhanced with CNTs as part of the network and mobilities are larger than that of pure Ag_2Te.

We mention that the effect of the irregularities in the nanoparticle positions and in the strengths of the tunneling coupling is different for metallic and insulating samples. If the coupling between the particles is sufficiently strong and the system is well-conducting, the irregularities are not very important.[51] In contrast, irregularities become crucial in the limit of low coupling, where the system is an insulator. The key

Table 1. Electrical Conductivity, Carrier Concentration, and Mobility of CNTs/Ag_2Te Hybrids and Pure Ag_2Te

	σ (S/m)	n (cm^{-3})	μ ($cm^2\ V^{-1}\ s^{-1}$)
CA-1	1.91×10^4	6.59×10^{18}	181.1
CA-2	8.10×10^3	2.05×10^{18}	246.7
CA-3	2.11×10^3	1.09×10^{18}	120.7
Ag_2Te	1.85×10^4	9.10×10^{19}	12.7

dx.doi.org/10.1021/am4059167 | ACS Appl. Mater. Interfaces 2014, 6, 4940−4946

parameter that determines most of the physical properties of inhomogeneous samples is the dimensional tunneling conductance g between neighboring particles. Samples with $g > 1$ exhibit metallic transport properties, while those with $g < 1$ show insulating behavior. All of our samples belong to the insulating side of the metal−insulator transition. Therefore, the charge on each particle becomes quantized as in the standard Coulomb blockade behavior. In this case, an electron has to overcome an electrostatic barrier of the order E_c to hop onto a neighboring particle, with E_c being the Coulomb energy of a single particle. At applied bias voltages and temperatures large enough to overcome local Coulomb energy costs, transport occurs by sequential tunneling between neighboring dots.[52] At small bias and low temperatures, sequential tunneling is suppressed by the Coulomb blockade. In this regime, conduction involves higher order tunneling processes, the so-called co-tunneling events, which can transport a charge over distances of several particles without incurring the full Coulomb energy costs. The above physics is valid for low temperatures, below 380 K. At higher temperatures, above 380 K, our samples show metallic behavior, meaning that the temperature reaches the size of the Coulomb gap. In this case, the number of electrons in the conducting band increases exponentially with the temperature, leading to metallic behavior: the higher the temperature, the lower the conductivity. This behavior is the consequence of the fact that the number of phonons increases with the temperature, leading to more difficult electron propagation through the sample because of many scattering events.

Seebeck coefficients of three CNTs/Ag_2Te hybrid buckypaper samples display n-type properties (negative Seebeck coefficient) (Figure 3B). Generally, the absolute values of Seebeck coefficients of three CNTs/Ag_2Te hybrid samples are larger at higher temperatures in the temperature range of ∼418−550 K. Among them, CA-1 exhibits the highest Seebeck value of 228 μV/K at 537 K. The two other hybrid samples, CA-2 and CA-3, also achieve Seebeck values of >100 μV/K when the temperature is higher than 480 K. The maximum Seebeck value obtained for the Ag_2Te pellet is 157 μV/K at 421 K, which is ∼100 K lower than that of CA-1. The CNT buckypaper shows a lower p-type value (∼30−50 μV/K) within the measured temperature range. The maximum Seebeck value of CA-1 is ∼45% higher than that of the pure Ag_2Te pellet and 4 times higher than that of pure CNT buckypaper. The enhancement of the Seebeck value for CA-1 may result from the change of the density of states because of the fact that the Ag_2Te dopants may generate some impurity levels in the band structures.

In combination of the Seebeck coefficient and electrical conductivity, the power factors of the CNTs/Ag_2Te hybrids, pure Ag_2Te, and pure CNTs are calculated (Figure 3C). Because of the largest Seebeck values and highest electrical conductivity, sample CA-1 presents the largest power factor compared to those of all of the other samples. The highest power factor of CA-1 is 579 μW m^{-1} K^{-2} at 537 K, which is 2 times that of the pure Ag_2Te pellet value and 80 times that of the pure CNT buckypaper value in the same temperature range.

Thermal conductivities (Figure 3D) of selected samples, CA-1, pure Ag_2Te, and pure CNTs were measured by laser flash. Sample CA-1 exhibits a low thermal conductivity of ∼0.7 W m^{-1} K^{-1}, which is lower than that of the pure Ag_2Te pellet and pure CNTs buckpaper in the same temperature range. Thermal conductivity, κ, can be expressed as $\kappa = \kappa_e + \kappa_L$, where κ_e and κ_L are electron thermal conductivity and lattice thermal conductivity, respectively. In the absence of inelastic processes, the electron thermal conductivity can be estimated using Wiedemann−Franz relation $\kappa_e = L\sigma T$. Because the Lorenz number cannot be accurately determined, the accurate value of κ_e cannot be confirmed. However, if we assume $L = 2.44 \times 10^{-8}$ W Ω K^{-2} and take the point of 525 K as an example, the electron thermal conductivity of CA-1, Ag_2Te, and CNT can be estimated as 0.14, 0.1, and 0.05 W m^{-1} K^{-1}, respectively. The lattice thermal conductivity can be calculated then as 0.55, 0.68, and 1.03 W m^{-1} K^{-1}, respectively. Although sample CA-1 has the highest electron thermal conductivity because of the largest electrical conductivity, it exhibits the lowest lattice thermal conductivity mainly attributed to the strong phonon scattering of the hybrid structure. It is worth noting here that the Ag_2Te sample is a dense pellet prepared by hot press at 673 K, while the CA-1 and pure CNTs samples are loosely packed buckypapers. The structural difference will also affect the lattice thermal conductivity. In general, the total thermal conductivity shows the non-monotonic temperature behavior because of competition between two different mechanisms. At high temperatures, the number of phonons is large leading to larger thermal conductivity.

If we do not consider the anisotropic aspect of such buckypaper, the figure of merit, ZT, can be calculated on the basis of the measured electric conductivities, Seebeck coefficients, and thermal conductivities. The estimated highest figure of merit, ZT, is 0.44 at 525 K on the sample CA-1. It is more than 2 times higher than that of pure Ag_2Te and 100 times higher than that of CNT. Although the TE performance of Ag_2Te-based materials may be further enhanced with more efforts (e.g., tuning particle size[53]), they are rigid and may have different working temperatures.[54] Hence, the CNTs/Ag_2Te hybrid holds niche applications because it is flexible and robust.

CONCLUSION

In summary, we successfully synthesized n-type CNTs/Ag_2Te hybrids via a solvothermal approach. The Ag_2Te particles attached on CNT bundles have a small size of ∼10 nm, and these CNTs/Ag_2Te hybrids can be prepared into flexible buckypaper. The hybrid sample CA-1 shows a higher electrical conductivity, higher Seebeck coefficient, and lower thermal conductivity than those of pure Ag_2Te and pure CNTs in the temperature range of 325−525 K. These enhancements may be attributed to the doping effect, more impurity levels, and stronger phonon scattering, respectively. Hence, its maximum ZT value of 0.44 is 2 times higher than that of the pure Ag_2Te pellet and 100 times higher than that of pure CNT buckypaper. This result shows that CNTs/Ag_2Te hybrids can be a promising new type n-type TE material with mechanical flexibility and acceptable ZT values.

ASSOCIATED CONTENT

Supporting Information

Schematic of the ZEM-3 setup (Figure S1) and thermal diffusivity and specific heat capacity results (Figure S2). This material is available free of charge via the Internet at http://pubs.acs.org.

AUTHOR INFORMATION

Corresponding Author

*E-mail: alexyan@ntu.edu.sg.

Notes

The authors declare no competing financial interest.

■ ACKNOWLEDGMENTS

The authors gratefully acknowledge Academic Research Fund (AcRF) Tier 1 RG 2/13 of Ministry of Education (MOE, Singapore), NRF2009EWT-CERP001-026 (Singapore), Agency for Science, Technology and Research (A*STAR) Science and Engineering Research Council (SERC) Grant 1021700144, and MPA 23/04.15.03 RDP 020/10/113 grants. The authors also gratefully acknowledge Republic Polytechnic, Singapore, for the laser flash measurements.

■ REFERENCES

(1) Snyder, G. J.; Toberer, E. S. Complex thermoelectric materials. *Nat. Mater.* **2008**, *7*, 105−114.
(2) Hochbaum, A. I.; Chen, R. K.; Delgado, R. D.; Liang, W. J.; Garnett, E. C.; Najarian, M.; Majumdar, A.; Yang, P. D. Enhanced thermoelectric performance of rough silicon nanowires. *Nature* **2008**, *451*, 163−168.
(3) Boukai, A. I.; Bunimovich, Y.; Tahir-Kheli, J.; Yu, J. K.; Goddard, W. A.; Heath, J. R. Silicon nanowires as efficient thermoelectric materials. *Nature* **2008**, *451*, 168−171.
(4) Nielsch, K.; Bachmann, J.; Kimling, J.; Bottner, H. Thermoelectric nanostructures: From physical model systems towards nanograined composites. *Adv. Energy Mater.* **2011**, *1*, 713−731.
(5) Xiao, C.; Xu, J.; Li, K.; Peng, J.; Yang, J. L.; Xie, Y. Superionic phase transition in silver chalcogenide nanocrystals realizing optimized thermoelectric performance. *J. Am. Chem. Soc.* **2012**, *134*, 4287−4293.
(6) Yang, C. C.; Li, S. A. Basic principles for rational design of high-performance nanostructured silicon-based thermoelectric materials. *ChemPhysChem* **2011**, *12*, 3614−3618.
(7) Heremans, J. P.; Jovovic, V.; Toberer, E. S.; Saramat, A.; Kurosaki, K.; Charoenphakdee, A.; Yamanaka, S.; Snyder, G. J. Enhancement of thermoelectric efficiency in PbTe by distortion of the electronic density of states. *Science* **2008**, *321*, 554−557.
(8) Venkatasubramanian, R.; Siivola, E.; Colpitts, T.; O'Quinn, B. Thin-film thermoelectric devices with high room-temperature figures of merit. *Nature* **2001**, *413*, 597−602.
(9) Poudel, B.; Hao, Q.; Ma, Y.; Lan, Y. C.; Minnich, A.; Yu, B.; Yan, X. A.; Wang, D. Z.; Muto, A.; Vashaee, D.; Chen, X. Y.; Liu, J. M.; Dresselhaus, M. S.; Chen, G.; Ren, Z. F. High-thermoelectric performance of nanostructured bismuth antimony telluride bulk alloys. *Science* **2008**, *320*, 634−638.
(10) Hsu, K. F.; Loo, S.; Guo, F.; Chen, W.; Dyck, J. S.; Uher, C.; Hogan, T.; Polychroniadis, E. K.; Kanatzidis, M. G. Cubic $AgPb_mSbTe_{2+m}$: Bulk thermoelectric materials with high figure of merit. *Science* **2004**, *303*, 818−821.
(11) Wang, R. Y.; Feser, J. P.; Lee, J. S.; Talapin, D. V.; Segalman, R.; Majumdar, A. Enhanced thermopower in PbSe nanocrystal quantum dot superlattices. *Nano Lett.* **2008**, *8*, 2283−2288.
(12) Ishiwata, S.; Shiomi, Y.; Lee, J. S.; Bahramy, M. S.; Suzuki, T.; Uchida, M.; Arita, R.; Taguchi, Y.; Tokura, Y. Extremely high electron mobility in a phonon-glass semimetal. *Nat. Mater.* **2013**, *12*, 512−517.
(13) Rhyee, J. S.; Lee, K. H.; Lee, S. M.; Cho, E.; Il Kim, S.; Lee, E.; Kwon, Y. S.; Shim, J. H.; Kotliar, G. Peierls distortion as a route to high thermoelectric performance in $In_4Se_{3-\delta}$ crystals. *Nature* **2009**, *459*, 965−968.
(14) Mishra, H.; Cola, B. A.; Rawat, V.; Amama, P. B.; Biswas, K. G.; Xu, X. F.; Fisher, T. S.; Sands, T. D. Thermomechanical and thermal contact characteristics of bismuth telluride films electrodeposited on carbon nanotube arrays. *Adv. Mater.* **2009**, *21*, 4280−4283.
(15) Bubnova, O.; Khan, Z. U.; Malti, A.; Braun, S.; Fahlman, M.; Berggren, M.; Crispin, X. Optimization of the thermoelectric figure of merit in the conducting polymer poly(3,4-ethylenedioxythiophene). *Nat. Mater.* **2011**, *10*, 429−433.
(16) Dubey, N.; Leclerc, M. Conducting polymers: Efficient thermoelectric materials. *J. Polym. Sci., Part B: Polym. Phys.* **2011**, *49*, 467−475.
(17) Kim, D.; Kim, Y.; Choi, K.; Grunlan, J. C.; Yu, C. H. Improved thermoelectric behavior of nanotube-filled polymer composites with poly(3,4-ethylenedioxythiophene) poly(styrenesulfonate). *ACS Nano* **2010**, *4*, 513−523.
(18) Sun, Y. M.; Sheng, P.; Di, C. A.; Jiao, F.; Xu, W.; Qiu, D.; Zhu, D. B. Organic thermoelectric materials and devices based on p- and n-type poly(metal 1,1,2,2-ethenetetrathiolate)s. *Adv. Mater.* **2012**, *24*, 932−937.
(19) Dillon, A. C.; Jones, K. M.; Bekkedahl, T. A.; Kiang, C. H.; Bethune, D. S.; Heben, M. J. Storage of hydrogen in single-walled carbon nanotubes. *Nature* **1997**, *386*, 377−379.
(20) Baughman, R. H.; Zakhidov, A. A.; de Heer, W. A. Carbon nanotubes—The route toward applications. *Science* **2002**, *297*, 787−792.
(21) Ebbesen, T. W.; Lezec, H. J.; Hiura, H.; Bennett, J. W.; Ghaemi, H. F.; Thio, T. Electrical conductivity of individual carbon nanotubes. *Nature* **1996**, *382*, 54−56.
(22) Ajayan, P. M. Nanotubes from carbon. *Chem. Rev.* **1999**, *99*, 1787−1799.
(23) Thostenson, E. T.; Ren, Z. F.; Chou, T. W. Advances in the science and technology of carbon nanotubes and their composites: A review. *Compos. Sci. Technol.* **2001**, *61*, 1899−1912.
(24) Coleman, J. N.; Khan, U.; Blau, W. J.; Gun'ko, Y. K. Small but strong: A review of the mechanical properties of carbon nanotube−polymer composites. *Carbon* **2006**, *44*, 1624−1652.
(25) Futaba, D. N.; Hata, K.; Yamada, T.; Hiraoka, T.; Hayamizu, Y.; Kakudate, Y.; Tanaike, O.; Hatori, H.; Yumura, M.; Iijima, S. Shape-engineerable and highly densely packed single-walled carbon nanotubes and their application as super-capacitor electrodes. *Nat. Mater.* **2006**, *5*, 987−994.
(26) Xia, Y. N.; Yang, P. D.; Sun, Y. G.; Wu, Y. Y.; Mayers, B.; Gates, B.; Yin, Y. D.; Kim, F.; Yan, Y. Q. One-dimensional nanostructures: Synthesis, characterization, and applications. *Adv. Mater.* **2003**, *15*, 353−389.
(27) Joachim, C.; Gimzewski, J. K.; Aviram, A. Electronics using hybrid-molecular and mono-molecular devices. *Nature* **2000**, *408*, 541−548.
(28) Yao, Q.; Chen, L. D.; Zhang, W. Q.; Liufu, S. C.; Chen, X. H. Enhanced thermoelectric performance of single-walled carbon nanotubes/polyaniline hybrid nanocomposites. *ACS Nano* **2010**, *4*, 2445−2451.
(29) Pettes, M. T.; Shi, L. Thermal and structural characterizations of individual single-, double-, and multi-walled carbon nanotubes. *Adv. Funct. Mater.* **2009**, *19*, 3918−3925.
(30) Berber, S.; Kwon, Y. K.; Tomanek, D. Unusually high thermal conductivity of carbon nanotubes. *Phys. Rev. Lett.* **2000**, *84*, 4613−4616.
(31) Akoshima, M.; Hata, K.; Futaba, D. N.; Mizuno, K.; Baba, T.; Yumura, M. Thermal diffusivity of single-walled carbon nanotube forest measured by laser flash method. *Jpn. J. Appl. Phys.* **2009**, *48*, No. 05EC07.
(32) Yu, C.; Choi, K.; Yin, L.; Grunlan, J. C. Light-weight flexible carbon nanotube based organic composites with large thermoelectric power factors. *ACS Nano* **2011**, *5*, 7885−7892.
(33) Meng, C. Z.; Liu, C. H.; Fan, S. S. A promising approach to enhanced thermoelectric properties using carbon nanotube networks. *Adv. Mater.* **2010**, *22*, 535−539.
(34) Zhao, W. Y.; Fan, S. F.; Xiao, N.; Liu, D. Y.; Tay, Y. Y.; Yu, C.; Sim, D. H.; Hng, H. H.; Zhang, Q. C.; Boey, F.; Ma, J.; Zhao, X. B.; Zhang, H.; Yan, Q. Y. Flexible carbon nanotube papers with improved thermoelectric properties. *Energy Environ. Sci.* **2011**, *5*, 5364−5369.
(35) Ma, Y.; Hao, Q.; Poudel, B.; Lan, Y. C.; Yu, B.; Wang, D. Z.; Chen, G.; Ren, Z. F. Enhanced thermoelectric figure-of-merit in p-type nanostructured bismuth antimony tellurium alloys made from elemental chunks. *Nano Lett.* **2008**, *8*, 2580−2584.

(36) Lan, Y. C.; Poudel, B.; Ma, Y.; Wang, D. Z.; Dresselhaus, M. S.; Chen, G.; Ren, Z. F. Structure study of bulk nanograined thermoelectric bismuth antimony telluride. *Nano Lett.* **2009**, *9*, 1419−1422.
(37) Zhou, W. W.; Zhu, J. X.; Li, D.; Hng, H. H.; Boey, F. Y. C.; Ma, J.; Zhang, H.; Yan, Q. Y. Binary-phased nanoparticles for enhanced thermoelectric properties. *Adv. Mater.* **2009**, *21*, 3196−3200.
(38) Heremans, J. P.; Thrush, C. M.; Morelli, D. T. Thermopower enhancement in lead telluride nanostructures. *Phys. Rev. B: Condens. Matter Mater. Phys.* **2004**, *70*, 115334.
(39) Biswas, K.; He, J. Q.; Zhang, Q. C.; Wang, G. Y.; Uher, C.; Dravid, V. P.; Kanatzidis, M. G. Strained endotaxial nanostructures with high thermoelectric figure of merit. *Nat. Chem.* **2011**, *3*, 160−166.
(40) Kim, P.; Shi, L.; Majumdar, A.; McEuen, P. L. Thermal transport measurements of individual multiwalled nanotubes. *Phys. Rev. Lett.* **2001**, *87*, 215502.
(41) Popov, V. N. Carbon nanotubes: Properties and application. *Mater. Sci. Eng., R* **2004**, *43*, 61−102.
(42) Zuev, Y. M.; Chang, W.; Kim, P. Thermoelectric and magnetothermoelectric transport measurements of graphene. *Phys. Rev. Lett.* **2009**, *102*, 096807.
(43) Xiao, N.; Dong, X. C.; Song, L.; Liu, D. Y.; Tay, Y.; Wu, S. X.; Li, L. J.; Zhao, Y.; Yu, T.; Zhang, H.; Huang, W.; Hng, H. H.; Ajayan, P. M.; Yan, Q. Y. Enhanced thermopower of graphene films with oxygen plasma treatment. *ACS Nano* **2011**, *5*, 2749−2755.
(44) Freeman, D. D.; Choi, K.; Yu, C. n-Type thermoelectric performance of functionalized carbon nanotube-filled polymer composites. *Plos One* **2012**, *7*, No. e47822.
(45) Yu, C. H.; Murali, A.; Choi, K. W.; Ryu, Y. Air-stable fabric thermoelectric modules made of n- and p-type carbon nanotubes. *Energy Environ. Sci.* **2012**, *5*, 9481−9486.
(46) Liu, J. H.; Miao, H. Y.; Saravanan, L.; Wang, L. C.; Tsai, R. H. Tuning of thermoelectric property in the flexible MWCNT bucky-paper. *Asian—J. Chem.* **2013**, *25*, S27−S29.
(47) Hu, C. H.; Liu, C. H.; Chen, L. Z.; Meng, C. Z.; Fan, S. S. A demo opto-electronic power source based on single-walled carbon nanotube sheets. *ACS Nano* **2010**, *4*, 4701−4706.
(48) Urban, J. J.; Talapin, D. V.; Shevchenko, E. V.; Kagan, C. R.; Murray, C. B. Synergismin binary nanocrystal superlattices leads to enhanced p-type conductivity in self-assembled PbTe/Ag_2Te thin films. *Nat. Mater.* **2007**, *6*, 115−121.
(49) Babel, A.; Jenekhe, S. A. High electron mobility in ladder polymer field-effect transistors. *J. Am. Chem. Soc.* **2003**, *125*, 13656−13657.
(50) Zhang, S. N.; Zhu, T. J.; Yang, S. H.; Yu, C.; Zhao, X. B. Improved thermoelectric properties of $AgSbTe_2$ based compounds with nanoscale Ag_2Te in situ precipitates. *J. Alloys Compd.* **2010**, *499*, 215−220.
(51) Beloborodov, I. S.; Efetov, K. B.; Lopatin, A. V.; Vinokur, V. M. Transport properties of granular metals at low temperatures. *Phys. Rev. Lett.* **2003**, *91*, 246801.
(52) Beloborodov, I. S.; Lopatin, A. V.; Vinokur, V. M.; Efetov, K. B. Granular electronic systems. *Rev. Mod. Phys.* **2007**, *79*, 469−518.
(53) Zhou, W. W.; Zhao, W. Y.; Lu, Z. Y.; Zhu, J. X.; Fan, S. F.; Ma, J.; Hng, H. H.; Yan, Q. Y. Preparation and thermoelectric properties of sulfur doped Ag_2Te nanoparticles via solvothermal methods. *Nanoscale* **2012**, *4*, 3926−3931.
(54) Fujikane, M.; Kurosaki, K.; Muta, H.; Yamanaka, S. Thermoelectric properties of α- and β-Ag_2Te. *J. Alloys Compd.* **2005**, *393*, 299−301.